ARL 69-0170
OCTOBER 1969

Aerospace Research Laboratories

HYPERSONIC WIND TUNNEL MEASUREMENTS OF ROLL DAMPING DERIVATIVES FOR CONES

OTTO WALCHNER
FRANK M. SAWYER
THOMAS A. DURHAM, CAPT, USAF
HYPERSONIC RESEARCH LABORATORY

Project No. 7064

OFFICE OF AEROSPACE RESEARCH
United States Air Force

NOTICES

When Government drawings, specifications, or other data are used for any purpose other than in connection with a definitely related Government procurement operation, the United States Government thereby incurs no responsibility nor any obligation whatsoever; and the fact that the Government may have formulated, furnished, or in any way supplied the said drawings, specifications, or other data, is not to be regarded by implication or otherwise as in any manner licensing the holder or any other person or corporation, or conveying any rights or permission to manufacture, use, or sell any patented invention that may in any way be related thereto.

Agencies of the Department of Defense, qualified contractors and other government agencies may obtain copies from the

Defense Documentation Center
Cameron Station
Alexandria, Virginia 22314

This document has been released to the

- - - - - - - - -

CLEARINGHOUSE
U.S. Department of Commerce
Springfield, Virginia 22151

for sale to the public.

Copies of ARL Technical Documentary Reports should not be returned to Aerospace Research Laboratories unless return is required by security considerations, contractual obligations or notices on a specified document.

400 - December 1969 - CO455 - 104-2275

ARL 69-0170

HYPERSONIC WIND TUNNEL MEASUREMENTS OF ROLL DAMPING DERIVATIVES FOR CONES

OTTO WALCHNER
FRANK M. SAWYER
THOMAS A. DURHAM, CAPT, USAF
HYPERSONIC RESEARCH LABORATORY

OCTOBER 1969

Project 7064

AEROSPACE RESEARCH LABORATORIES
OFFICE OF AEROSPACE RESEARCH
UNITED STATES AIR FORCE
WRIGHT-PATTERSON AIR FORCE BASE, OHIO

FOREWORD

This technical report was prepared by the Hypersonic Research Laboratory of the Aerospace Research Laboratories under Project 7064 entitled "High Velocity Fluid Mechanics" and is the final report on hypersonic roll damping measurements on slender, blunted, cones in ARL's 20-inch hypersonic wind tunnel. The report includes a comparison of the experiments with recently published theoretical solutions.

ABSTRACT

The roll damping derivatives, C_{ℓ_p}, for a 10^o cone with various nose bluntness ratios were measured in ARL's 20-inch hypersonic wind tunnel at Mach 12.7 and 14.2, $Re_{d\infty} = 2.5 \times 10^5$, in axial flow and at angles of attack up to ± 8 degrees. An air bearing, supporting the model with freedom in roll, was designed specifically for these tests. The bearing performance is described in detail. The measured derivatives compare very favorably with Quinn's laminar roll damping theory for blunted cones in axial flow. A moderate decrease of the magnitude of C_{ℓ_p} results from blunting the nose. At angles of attack, this blunt nose effect diminishes and the blunt cone derivatives approach the sharp cone values with increasing angle of attack. Experimental difficulties at angles of attack were traced to possible free stream deficiencies and were overcome by increasing the model roll rate. No effect of the reduced roll rate on the damping derivative at zero angle of attack was found within the range $pd/2U_\infty = 0.003$ to 0.021.

TABLE OF CONTENTS

LIST OF ILLUSTRATIONS

LIST OF SYMBOLS

A, B, C	Constants, Eq (4), (5)
C_1	clearance, journal bearing
C_2	clearance, thrust bearing
d	base diameter, cone model
I	moment of inertia with respect to roll axis
k	friction moment parameter, bearing
L	rolling moment, positive clockwise when looking from base to nose
L_B	roll-moment, bearing
L_T	driving torque, bearing
ℓ	journal length
M	Mach number
p	roll rate, positive clockwise, when looking from base to nose
P	pressure
P_s	air supply pressure, bearing reservoir
P_t	total pressure, wind tunnel
P_∞	free stream pressure, wind tunnel

P_B	base pressure, cone model
$q = \frac{\rho_\infty U_\infty^2}{2}$	dynamic pressure, wind tunnel
r_N	nose radius, model
r_B	base radius, model
R_1	journal radius, bearing
R_2	inside radius, thrust plate
$Re_{d,\infty}$	Reynolds number with respect to base diameter and free stream conditions
S	base area, cone model
T	roll period
T_t	total temperature, wind tunnel
U_∞	free stream velocity
α	angle of attack
γ	ratio of specific heats
ϵ	eccentricity ratio, air bearing
θ	cone half-angle
μ	coefficient of viscosity
ρ_∞	free stream density
$C_\ell = \frac{L}{qSd}$	rolling moment coefficient

$$C_{\ell_p} = \frac{\partial C_\ell}{\partial\left(\frac{pd}{2U_\infty}\right)}$$ roll damping derivative

$(\dot{\ })$ time derivative

$(\ )_j$ refer to journal bearing

$(\ )_t$ refer to thrust bearing

SECTION I

INTRODUCTION

The roll damping derivative, C_{ℓ_p}, is one of the many aerodynamic coefficients which influence the flight dynamics of a rolling vehicle. It was learned at the Second Technical Workshop on Dynamic Stability Testing, held at AEDC, 1965, that very limited knowledge exists of this derivative for conical configurations at high Mach numbers. Consequently, a program was initiated at ARL with the purpose of making a contribution in this area. First, the roll damping moment was estimated for a 10^{o} pointed cone model in ARL's 20-inch hypersonic wind tunnel. Next, an externally pressurized air bearing was designed to support the cone model in the wind tunnel, with freedom in roll, so that the bearing friction moment was smaller than the aerodynamic moment to be measured. For a series of nose bluntness ratios, the roll damping derivatives were measured for axial flow conditions and over a limited range of angles of attack at Mach 12.75 and 14.25.

Parallel to the experimental program, Quinn started a theoretical program to compute the laminar roll damping derivatives of spherically blunted cones by means of the boundary layer theory. Quinn's theory has been published and was presented, with the first experimental results, at the Third Technical Workshop on Dynamic Stability Problems held at NASA, Ames, 1968.

The present report summarizes the experimental effort, including the investigation of the air bearing characteristics.

SECTION II

DISCUSSION

1. APPARATUS

a. Wind Tunnel

The ARL twenty-inch diameter hypersonic wind tunnel is an open jet, blow-down, air facility with a contoured axisymmetric nozzle. Interchangeable throat sections provide for Mach number variation. Detailed descriptions of this wind tunnel and its operating characteristics are contained in Reference 1.

Typical test conditions for the present study are:

M_∞	P_t (psia)	T_t (^oR)	Re_∞/ft
12.75	1185	2010	6.3×10^5
14.25	1615	2080	5.8×10^5

The core of the free stream is approximately 10 inches in diameter. Various calibration and liquefaction studies indicate that the air in the test section is supersaturated but not liquefied (Reference 2).

b. Model

The model is a 10-degree semivertex angle cone with an open base of 4.95 inches in diameter. The model consists of a thin-walled (0.050 in.) magnesium alloy body with provision for interchanging ten different aluminum alloy noses. The bluntness ratios of the hemispherically blunted noses range from $r_N/r_B = 0.010$ to 0.350. The nose cavity is vented to the open base of

the model. The surface roughness of the cone body and noses is less than ten microinches, rms. It was intended that the model be concentric with the roll axis within 0.001 inch; however, the eccentricity actually varies from 0.001 inch at the nose to 0.005 inch at the base.

The moments of inertia, with respect to the roll axis, were measured with a torsion pendulum. For the bearing rotor assembly, without the model, $I = 2.51 \times 10^{-5}$ ft-lb-sec^2. For the cone rotor assembly, with $r_N/r_B = 0.01$, $I = 1.99 \times 10^{-3}$ ft-lb-scc^2. The moments of incrtia for the model with the other noses were only slightly different. The model was not dynamically balanced. A small static unbalance was noted but was not corrected.

c. Support System

The cone model, air bearing, sting, strut system and associated equipment are shown in Figure 1. The cone model is mounted on the forward end of the rotor shaft. The model is spun up with an electric motor connected to the clutch by a flexible cable, gears, and shaft. The clutch is engaged by energizing the solenoid and is disengaged by a spring. The rotor coupling contains two permanent magnets which, in conjunction with the pickup coil in the sting, generate the signal for measuring the roll period.

Dry air from the facility's high-pressure air supply was passed through a 4-micron filter before entering the bearing reservoir. The reservoir pressure was 255 psia. Approximately 85% of the flow through the bearing is discharged through the sting and strut into the vacuum line downstream of the diffuser. The rest, however, escapes through the clearance between the rotor shaft and the front thrust plate into the wake of the cone model.

d. Air Bearing

Mechanical details and performance characteristics of the bearing are described in the Appendix.

e. Instrumentation

The roll period, T, was measured with an electronic counter, which averaged ten consecutive cycles of signal oscillation, and the result, equal to one-half of the model roll period (because of the two magnets), is printed by a digital recorder. A second counter generated a time signal which was also printed by the recorder. Thus a record of T/2 as a function of time was available immediately after each run.

2. EXPERIMENTAL METHOD

The roll damping data were obtained by employing the spin decay technique. This method consists of driving the model up to the required roll rate, disengaging and stopping the drive, and recording the roll period as a function of time. The wind-on run was preceded and followed by a wind-off vacuum tare run.

The equations of motion are

$$(I\dot{p})_{\text{wind-on}} = C_{\ell_p} \frac{pd}{2U_\infty} qSd + L_B(p, P_s)$$

and

$$(I\dot{p})_{\text{wind-off}} = L_B(p, P_s)$$

The roll damping derivative is, therefore,

$$C_{\ell_p} = \frac{4I}{\rho_\infty U_\infty Sd^2} \left[\left(\frac{\dot{p}}{p} \right)_{\text{wind-on}} - \left(\frac{\dot{p}}{p} \right)_{\text{wind-off}} \right]$$

or, by introducing the roll period, $T = 2\pi/p$,

$$C_{\ell_p} = -\frac{4I}{\rho_\infty U_\infty S d^2}\left[\left(\frac{\dot{T}}{T}\right)_{\text{wind-on}} - \left(\frac{\dot{T}}{T}\right)_{\text{wind-off}}\right]$$

The roll damping derivative is determined by the observed time history of the roll period and by known model constants and wind tunnel flow properties.

Analysis of the bearing performance (Appendix A) shows that the bearing moment, L_B, consists of a friction moment and a driving torque. For a given bearing temperature, the friction moment is proportional to the roll rate whereas the driving torque was found to depend on the bearing reservoir pressure and the roll rate. Care was therefore taken to make the wind-on and wind-off runs at identical supply pressures and over identical ranges of roll rate.

To minimize the aerodynamic roll damping moment in still air during the tare runs, the test cabin was evacuated to a pressure of 2 mm Hg.

The base pressure was monitored for every run since 15% of the air flow through the bearing dumps into the wake of the cone model. For comparison, the base pressure was also measured when the model was not rolling and there was no flow through the bearing.

In a separate series of runs, the cone surface temperature over the rear half of the rolling model was determined with temperature-sensitive paints (Tempilac). These data were needed for the theoretical computation of C_{ℓ_p}.

Model positions greater than ± 8 degrees of angle of attack were not investigated. The wind tunnel blockage by model and suspension system increased with angle of attack to such a degree that the pressure in the test cabin, surrounding the free stream, started to fluctuate when $\alpha \sim \pm 9$ degrees.

3. TEST RESULTS

The measured roll damping derivative, C_{ℓ_p}, for axial flow conditions at various reduced roll rates are presented in Figures 2, 3 and 4 for Mach 14.25 and 12.75. The experimental data are compared with theoretical predictions by Quinn[3, 4, 5]. For the specified test conditions, the laminar theory is seen to agree very well with the experiments. Only for larger bluntness ratios, $r_N/r_B > 0.3$, theory and experiment seem to deviate trendwise. Quinn has explained this effect by the simplifying approximations of his theory. A moderate but distinct decrease of the magnitude of the roll damping derivative results from increasing the nose bluntness. This effect is due to the change of the flow conditions at the outer edge of the boundary layer brought about by the swallowing of the blunt body entropy layer.

Figures 5 and 6 show test results at angles of attack up to ± 8 degrees for two bluntness ratios, r_N/r_B = 0.01 and 0.15, and for the reduced roll rate $pd/2U_\infty$ = 0.005. The roll damping derivative, C_{ℓ_p}, was expected to change with angle of attack but this change should be symmetrical at positive and negative angles of attack. The test did not produce the expected symmetry but it is seen that one set of test data for one roll direction is in near mirror symmetry with the test results for the other roll direction. This anomaly is believed to result from slight imperfections of the windstream such as swirl or side flow component or both together. Further studies are necessary for a satisfactory explanation of the observed asymmetry. For the present, the problem was overcome by an increase of the model roll rate. Figures 7 and 8 show that the larger roll rate, $pd/2U_\infty$ = 0.021, almost eliminates the previously observed asymmetry with angle of attack, but an asymmetrical trend can still be seen. The average values of the test data for both roll directions, from Figures 7 and 8, are considered to give the correct effect of angles of attack on C_{ℓ_p} at zero yaw. These average values are shown in Figure 9 and it is evident that the value of C_{ℓ_p} increases with angle of attack and that the C_{ℓ_p} values of the blunt cone approach the sharp cone values when the angle of attack increases. This trend is expected on the basis of the "tangent cone" concept. The tangent cone approximation assumes that the pressure distribution, along the windward ray of a cone at angle of attack, is nearly identical to the pressure distribution observed in axial flow over a "tangent cone" having the half angle $\theta + \alpha$. For a given nose radius, the bluntness

ratio of the equivalent tangent cone is therefore smaller than the bluntness ratio of the actual cone model. The pressure distribution along the windward ray of a blunt cone is therefore expected to approach the sharp cone pressure distribution as the angle of attack increases. At angles of attack it is the windward area which furnishes the main contribution to the roll damping moment. Therefore, the derivative, C_{ℓ_p}, for a blunt cone at an angle of attack should approach the C_{ℓ_p} of a sharp cone at the same angle of attack.

Comparing the test data for $\alpha = 0$ from Figures 5 to 8 with the data for the respective bluntness ratios shown in Figures 2 and 3, it is seen that a variation of the reduced roll rate from 0.003 to 0.021 has no effect on C_{ℓ_p}. This observation confirms the linear dependence of the rolling moment on the roll rate which is predicted by the theory.

Typical base pressure measurements are shown in Figure 10. The base pressure is relatively large, obviously due to suspension interference; however, it is believed that these base pressures were not large enough to alter the flow over the cone model. It is also seen from Figure 10 that the base pressure is only slightly increased by the portion of the bearing flow escaping into the wake of the cone model.

For run times of approximately 15 seconds, the following approximate wall temperatures at the rear portion of the model were determined with Tempilac paints:

$$T_w/T_t = 0.31 \text{ for } M_\infty = 14.25,\ T_t = 2010^\circ \text{ R}$$

$$T_w/T_t = 0.33 \text{ for } M_\infty = 12.75,\ T_t = 2080^\circ \text{ R}$$

High accuracy in determination of the wall temperature is not required for the theoretical computations since an error in T_w is nearly compensated by a corresponding change of the coefficient of viscosity.

REFERENCES

1. Gregoreck, G. M. and Lee, J. D., "Design Performance and Operational Characteristics of the ARL Twenty-Inch Hypersonic Wind Tunnel," ARL 62-392, August 1962.

2. Daum, F. L., "Air Condensation in a Hypersonic Wind Tunnel," AIAA Journal, Vol. 1, No. 9, May 1963.

3. Quinn, B., "The Hypersonic Roll Damping Derivative of a Blunt Cone," ARL 68-0137, July 1968.

4. Quinn, B., "The Laminar Hypersonic Roll Damping Derivative of a Blunt Cone," Transactions of the 3rd Technical Workshop on Dynamic Stability Problems, Nov 4-7, 1968, NASA Ames Research Center, Vol. III, Paper 1.

5. Quinn, B., "Blunt-Cone Roll-Damping Derivative," AIAA Journal, Vol. 7, No. 1, January 1969, pp 175-177.

6. Walchner, O., "Laminar Hypersonic Roll Damping Derivatives for a 10^{o} Cone," AIAA Journal, Vol. 7, No. 2, February 1969, pp 342-343.

7. Lund, J. W., "Gas Bearing Design Charts," Vol. 2, "The Hydrostatic Gas Journal Bearing and The Hydrostatic Gas Thrust Bearing," Mechanical Technology Incorporated, Latham, N. Y., No. MTI-65 TR5-II, Vol. 2, April 1965, AD 615920.

8. Wilson, R. E., "Real Gas Laminar Boundary Layer Skin Friction and Heat Transfer," Journal of the Aerospace Sciences, Vol. 29, No. 6, June 1962, pp 640-647.

9. Sims, J. L., "Tables for Supersonic Flow Around Right Circular Cones at Zero Angle of Attack," SP-3004, 1964, NASA.

10. Reinecke, W. G., "Charts for Use with Hypersonic Air Wind Tunnels," ARL 64-56, April 1964.

APPENDIX A.

DESIGN AND PERFORMANCE CHARACTERISTICS OF THE AIR BEARING

1. Design

The measurement of the roll damping of a cone model in the ARL 20-inch HWT at Mach 14 necessitated the use of a gas lubricated bearing which would have a low friction moment, large stiffness, small rate of exhaust flow, and a stable mode of motion in roll.

The design of the bearing was based on an estimate of the aerodynamic roll damping moment to be measured. For the wind tunnel flow conditions at Mach 14 and a 10^{o} cone with a base diameter of 5 inches, a roll damping moment per unit of roll-rate of -1.4×10^{-6} (ft-lb)/(rad/sec) was computed[6]. Reasonable accuracy of the roll damping measurements was expected with a bearing having a friction moment per unit of roll rate of about one-half of this value and the bearing was designed accordingly, using the design charts by Lund[7]. Designing for a lower friction moment was rejected since this could only be achieved by sacrificing bearing stiffness.

The bearing is externally pressurized (hydrostatic gas bearing) and has two journals and two thrust bearings. Inherently compensating flow restrictors were chosen to provide stiffness and to avoid the phenomenon of pneumatic hammer. Each journal is one inch in diameter and two inches long. The design clearances are C_1 = .0009 inch for the journal and C_2 = .001 inch for the thrust bearing. The lubricating air flow is admitted to each journal through 16 feeding holes located in a single plane and through 16 feeding holes in each thrust bearing. All feeding holes have a diameter of .016 inch. For an air supply pressure of 255 psia the bearing characteristics, computed from Reference 7, are:

Air flow rate	.017 lb/sec
Thrust stiffness	39,800 lb/in.
Radial stiffness	214,000 lb/in.
Pitch stiffness	482,000 in.-lb/rad
Friction moment per unit of roll rate	-0.81×10^{-6} (ft-lb)/(rad/sec)

The primary reason for the desired large stiffness values is the fact that the evaluation of the roll damping derivative, C_{ℓ_p}, depends on the difference between the wind-on and wind-off rolling moments of the cone-bearing assembly. Since there is no way to measure the bearing friction moment under the exact load conditions prevailing during the wind-on run, it is essential that the bearing friction moment be insensitive to load. This is accomplished by minimizing the rotor eccentricity due to load. According to Reference 7, the radial load and thrust load effects on the bearing moment are expressed by the factors

$$\left(1 - \epsilon_j^2\right)^{-1/2} \text{ and } \left(1 - \epsilon_t^2\right)^{-1}, \text{ respectively, where } \epsilon = \frac{\text{load/stiffness}}{\text{clearance}}.$$

Fortunately, in this respect, the dynamic pressure of the wind tunnel flow is small, q = 1/2 psi, and the aerodynamic loads are correspondingly small also (e.g., 3.5 lbs of lift at $\alpha = 10^{\circ}$). The above load factors are very nearly equal to unity so that load effects on the bearing moment are practically nonexistant. The bearing friction moments observed during the wind-off runs are therefore considered to represent accurately the bearing friction moment under wind-on conditions.

2. Mechanical Details

Details of the mechanical design are presented in Figure 11. The major components of the bearing are the journal and shaft, the bearing cylinder, two thrust plates, a housing, coupling and cover, ten vent plugs, two in the center of the bearing and four at each end and a number of "O" ring seals.

All of the metal parts were fabricated of stainless steel except for the cover which was made of aluminum alloy. The journal, bearing cylinder and thrust plates were made of 440 C stainless steel alloy and were heat treated to obtain dimensional stability and a hardness in the range of Rockwell C-55 to C-60.

The finished components were carefully measured and the following conditions were determined. The surface roughness of all of the bearing surfaces was less than 10 microinches rms. The thrust surfaces on the journal and thrust plates were flat within .000035 inch and, on assembly, adjacent surfaces were parallel within ± 1/2 minute of angle. All of the feeder holes measured .016 ± .001 inch in diameter. The journal and cylinder surfaces were round within 40 microinch. All except two of the radial feeding hole centerlines were equally spaced within the design tolerance of ± 1/2 degree. The angular spacing of the centerlines for these two adjacent holes exceeded the tolerance by +9 minutes and -14 minutes of angle. No attempt was made to measure a possible deviation of the feeding hole centerlines from a true radial direction. The clearance between thrust surfaces, with the journal centered, is .00095 inch. The radial clearance could not be determined over the full journal length. Measurements to a depth of 3/4 inch at each end of the bearing cylinder indicated a clearance of .00085 inch. The edges of the thrust feeding holes, at the thrust surface, were visually inspected with the aid of a 10 power microscope and were all found to be reasonably sharp and free of significant defects. A similar inspection of the radial feeding hole junctions was not possible due to their inaccessibility.

The high pressure air supply for the bearing passes through the coupling inlet into the annular space between the bearing cylinder and the housing and then through the feeding holes and across the bearing surfaces. Half of the flow across the thrust plates (about 15% of the total flow through the bearing) escapes between the forward thrust plate and the journal shaft. The balance of the flow through the bearing escapes through the four small vent plugs at each end and the two large vent plugs in the center of the assembly. The bearing cover forces this air to flow through radial holes in the coupling from which it is allowed to escape along the shaft.

3. Experimental Evaluation of the Bearing Performance

A comprehensive test program in which all of the computed design parameters were experimentally evaluated was not attempted. Instead, experiments were conducted to quantitatively evaluate the friction parameter and to qualitatively evaluate the stiffness.

The friction moment characteristics were determined from tests in still air at an ambient pressure of 2 mm Hg. The journal assembly, without cone model, was driven up to the desired angular speed. The drive mechanism was then disengaged and stopped, and the time history of the roll period was observed.

The equation of motion for the bearing under these conditions is

$$I\dot{p} = 2L_j + 2L_t$$

where, from Reference 7,

$$L_j = -2\pi\mu\ell R_1^3 C_1^{-1} p (1 - \epsilon_j^2)^{-1/2}$$

$$L_t = -(\pi/2)\mu R_1^4 C_2^{-1} p \left[1 - (R_2/R_1)^4\right] (1 - \epsilon_t^2)^{-1}$$

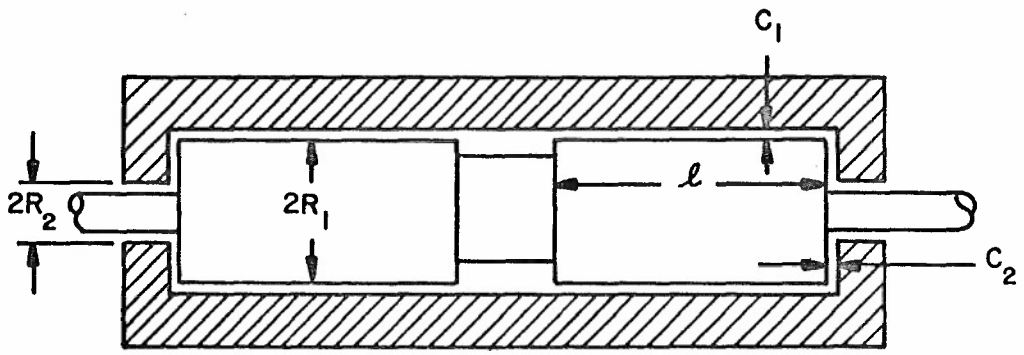

The first of these expressions (for $\epsilon = 0$) represents the exact solution for a laminar flow, which develops between two concentric cylinders of length, ℓ, when the inner cylinder, radius R_1, rotates at the rate, p, while the outer cylinder, radius $(R_1 + C_1)$, is at rest. The use of this expression for the externally pressurized bearing therefore neglects the effects of the flow through the bearing, especially the entrance effects near the feeding holes. The same holds for the second expression which, for $R_2 = 0$, is the friction moment acting on one side of a disc, of radius R_1, rotating in a housing having the small clearance C_2.

The roll equation of motion can now be written as $I\dot{p} = kp$, where, for $\epsilon = 0$

$$k = -\pi \mu R_1^3 \left\{ 4\frac{\ell}{C_1} + \frac{R_2}{C_2}\left[1 - \left(\frac{R_2}{R_1}\right)^4 \right] \right\} \qquad (1)$$

For a temperature of the lubricating air film of $T = 530$ R, the viscosity coefficient is $\mu = 38 \times 10^{-8}$ lb sec/ft^2. With the following bearing dimensions,

ℓ	R_1	R_2	C_1	C_2	
2.000	0.4994	0.200	0.0009	0.0010	inches

the expected value for the bearing friction parameter is

$$k = -0.81 \times 10^{-6} \text{ ft lb sec}$$

In the absence of a model and with no moments other than the friction moment acting on the bearing, the equation of motion yields the relation

$$\frac{k}{I} = \frac{\dot{p}}{p} = \frac{d(\dot{p})}{dp} = \text{constant}$$

The tests with no model attached to the rotor, however, did not support this relation. Figure 12 shows the observed roll acceleration, $\dot{p}$, as a function of the roll rate, p, for three different supply pressures and the following experimental facts are noted:

a. The roll acceleration varies linearly with the roll rate but the slope, $d(\dot{p})/dp$, is clearly a function of the supply pressure, P_s.

b. At zero roll rate, there is a positive roll acceleration, $\dot{p}_o$, which increases in proportion to the supply pressure. This means that the flow through the bearing somehow creates an aerodynamic driving torque, L_T, which forces the rotor to autorotate in a positive direction, $(p > 0)$.

c. The autorotation rate, p_a, is defined by the condition $\dot{p} = 0$. For $p = p_a$, the friction moment, kp_a, is balanced by the driving torque. The tests indicate that the autorotation roll rate increases when the supply pressure increases.

d. There is one distinctive roll rate, p_1, for which $\dot{p}$ has one and the same value for all supply pressures. This implies that the driving torque is not only a function of the supply pressure but must also be a function of the roll rate such that the driving torque vanishes for $p = p_1$. Any windmill shows a decrease of the torque coefficient when the roll rate increases and the roll rate for which the torque coefficient vanishes depends only on the geometry of the windmill for a given wind speed.

The difference between the expected and observed performance may now be explained as follows. For the obviously existing driving torque, L_T, a linear function of roll rate is assumed which satisfies the two observed conditions: $L_T = I\dot{p}_o$ at $p = 0$ and $L_T = 0$ for $p = p_1$.

That is,

$$L_T = I\dot{p}_o (1 - p/p_1) .$$

The roll equation for the rotor now becomes

$$I\dot{p} = kp + I\dot{p}_o (1 - p/p_1) . \tag{2}$$

Differentiating with respect to p gives the bearing friction parameter

$$k = I \left[\frac{d(\dot{p})}{dp} + \frac{\dot{p}_o}{p_1} \right] . \tag{3}$$

Tests with eight different supply pressures, from 36 to 288 psia, gave the values of $d(\dot{p})/dp$ and $\dot{p}_o$ shown in Figure 13. It is seen that these experimental data can closely be fitted by the following linear functions of the supply pressure, P_s.

$$\dot{p}_o = AP_s \tag{4}$$

$$\frac{d(\dot{p})}{dp} = - (B + CP_s) \tag{5}$$

where, from Figure 13,

$$A = 124.7 \times 10^{-4} \frac{\text{rad/sec}^2}{\text{psi}}$$

$$B = 313 \times 10^{-4} \frac{\text{rad/sec}^2}{\text{rad/sec}}$$

$$C = 0.666 \times 10^{-4} \frac{\text{rad/sec}^2}{(\text{rad/sec})\ \text{psi}}$$

Expressing the roll acceleration $\dot{p}$ by

$$\dot{p}(p) = \dot{p}_o + \frac{d(\dot{p})}{dp} p$$

$$= (A - Cp) P_s - Bp$$

it can be seen that $\dot{p}$ is independent of the bearing supply pressure for the one specific roll rate

$$p_1 = A/C . \tag{6}$$

Inserting Equations (4), (5) and (6) into (3) then gives the bearing friction parameter

$$k = -IB$$

Introducing $I = 0.251 \times 10^{-4}$ ft-lb-sec^2 and $B = 313 \times 10^{-4}$ sec^{-1}, obtain

$$k = -0.786 \times 10^{-6} \text{ ft-lb-sec.}$$

This value is independent of roll rate and supply pressure, as it should be, and agrees closely with the design information from Reference 7, as expressed by Equation (1).

The autorotation rate can also be computed from the assumed linear variation of the driving torque and compared with the observations. The autorotation roll rate corresponds to the condition $\dot{p} = 0$.

From Equation (2)

$$k\,p_a + I\dot{p}_o\,(1 - p_a/p_1) = 0$$

Introducing $\dot{p}_o = AP_s$, $p_1 = A/C$, $k = -IB$, obtain

$$p_a = \frac{AP_s}{B + CP_s} \tag{7}$$

It can be seen in Figure 14 that the autorotation rates obtained from Equation 7 are in close agreement with the observed values. Evidently, the assumed linear variation of the driving torque with roll rate is justified and explains the observed performance satisfactorily. It is believed that the driving torque is the result of undetected small machining asymmetries in the bearing components which cause an unsymmetrical flow within the lubricating film.

Introducing the roll period, $T = 2\pi/p$, which is the quantity measured during the tests, Equation (2) may be rewritten to obtain

$$I\frac{\dot{p}}{p} = -I\frac{\dot{T}}{T} = k + L_{T_o}\,(T - T_1)\,/\,2\pi \tag{2a}$$

where the bearing friction parameter, k, is independent of roll rate and supply pressure, L_{T_o} is the driving torque at zero roll rate, which varies with the supply pressure, and T_1 is the fixed roll period for which the driving torque vanishes at all supply pressures. According to Equation (2a), the term $I\dot{T}/T$ is expected to vary linearly with the roll period, T, at a given supply pressure. Tests of the journal alone (cone model detached) in still air, at an ambient pressure of 2 mm Hg., confirmed this linear relation over a wide range of roll periods (Figure 15). For the cone-journal assembly, however, this linearity exists only for $T \geq .045$ seconds and the value of $I\dot{T}/T$ is considerably

greater than the corresponding value obtained from the journal alone tests. This increase in $\dot{I}T/T$ between model-on and model-off tests is not fully understood. Approximately half of the increase was determined to be caused by the air exhausting between the forward thrust plate and the journal shaft. This flow, acting on the inner surfaces of the cone, produces an additional damping moment. The other half of the increase may be due to the known dynamic imbalance of the cone-journal assembly. For $T < .045$ seconds, the existance of several critical roll rates is obvious (Figure 15).

Two sets of wind tunnel tests were carried out to verify the predicted independence of the bearings' friction moment from the effects of aerodynamic forces and moments acting on the cone model and to check the adequacy of the bearings' stiffness. Figure 16 shows the results of tests at six different roll rates and at zero angle of attack. The values for $\dot{I}T/T$ for wind-on and wind-off conditions are seen to differ by a constant amount even near the critical speeds. The aerodynamic contribution to $\dot{I}T/T$ is constant because the derivative, C_{ℓ_p}, is independent of roll rate. The observed constant difference in $\dot{I}T/T$ therefore indicates that the bearing friction moment is independent of the aerodynamic load. Although roll damping tests near the critical speeds appear to be feasible, these critical roll rates were avoided for quantitative roll damping measurements.

The bearing stiffness increases with the supply pressure. The second set of tests was therefore made with different supply pressures ranging from 65 to 415 psia and at positive and negative angles of attack of 8 degrees. The bearing load at $\alpha = +8$ degrees is approximately one quarter of the load at $\alpha = -8$ degrees since the aerodynamic lift changes its direction at positive and negative angles of attack but the gravitational load does not. The data were reduced to yield the roll damping coefficient for the cone model. No dependence of C_{ℓ_p} on the supply pressure was detected for these extreme test conditions and it was concluded that the stiffness is adequate for tests at Mach 12 and 14 and at angles of attack ranging from +8 degrees to -8 degrees with a bearing supply pressure of 255 psia.

No evidence of unstable journal motion of the type characterized by pneumatic hammer or lockup was observed.

APPENDIX B.

THEORETICAL ROLL DAMPING DERIVATIVE FOR A POINTED CONE AT $a = 0$

The present study shows that the laminar roll damping derivative for a 10^{o} cone with various nose bluntness ratios is well predicted by Quinn's theory.[3, 4, 5] In practice, small bluntness ratios of $r_N/r_B < 0.1$ are of main interest today. Wind tunnel experiments in the continuum flow regime and theory indicate that spherical nose blunting of this order has little effect on the magnitude of C_{ℓ_p}. For this reason, the theoretical value of C_{ℓ_p} for a pointed cone is repeated here in a convenient form not explicitely expressed so in the referenced literature.

For zero angle of attack and laminar flow over a pointed cone, the theoretical roll damping derivative, as defined in this report, is given by the expression

$$C_{\ell_p} = -\frac{0.688}{(\sin\theta)^{1/2}\,(Re_{d,\infty})^{1/2}} \left[\lambda \frac{\mu_1}{\mu_\infty}\frac{P_1}{P_\infty}\frac{M_1}{M_\infty}\left(\frac{T_\infty}{T_1}\right)^{1/2}\right]^{1/2}$$

where, from Reference 8,

$$\lambda = \frac{T_1}{\mu_1}\frac{\mu'}{T'}$$

$$\frac{T'}{T_1} = 1 + 0.076\,(\gamma - 1)\,M_1^{\,2} + 0.481\,[\,(T_w/T_1) - 1\,]$$

and $\mu' = \mu(T')$

$\mu_\infty = \mu(T_\infty)$

$\mu_1 = \mu(T_1)$

$( )_w$ refers to wall condition;

$( )_\infty$ refers to free stream condition;

$( )_1$ refers to conditions at the outer edge of the boundary layer for which the inviscid surface values, available from conical flow tables[9], are substituted in Quinn's theory;

$( )'$ refers to average values through the boundary layer[8]

The coefficients of viscosity,[10] in lb-sec/ft^2, are

$$\mu = 2.27 \times 10^{-8} \frac{T^{3/2}}{T + 198.6}, \text{ (Sutherland, for } T \geq 180^{\circ} \text{ R)}$$

$$\mu = 10^{-8} (0.887 + 0.0663T + 0.0000589T^2), \text{ (Bromley \& Wilke, for } T \leq 180^{\circ} \text{ R)}$$

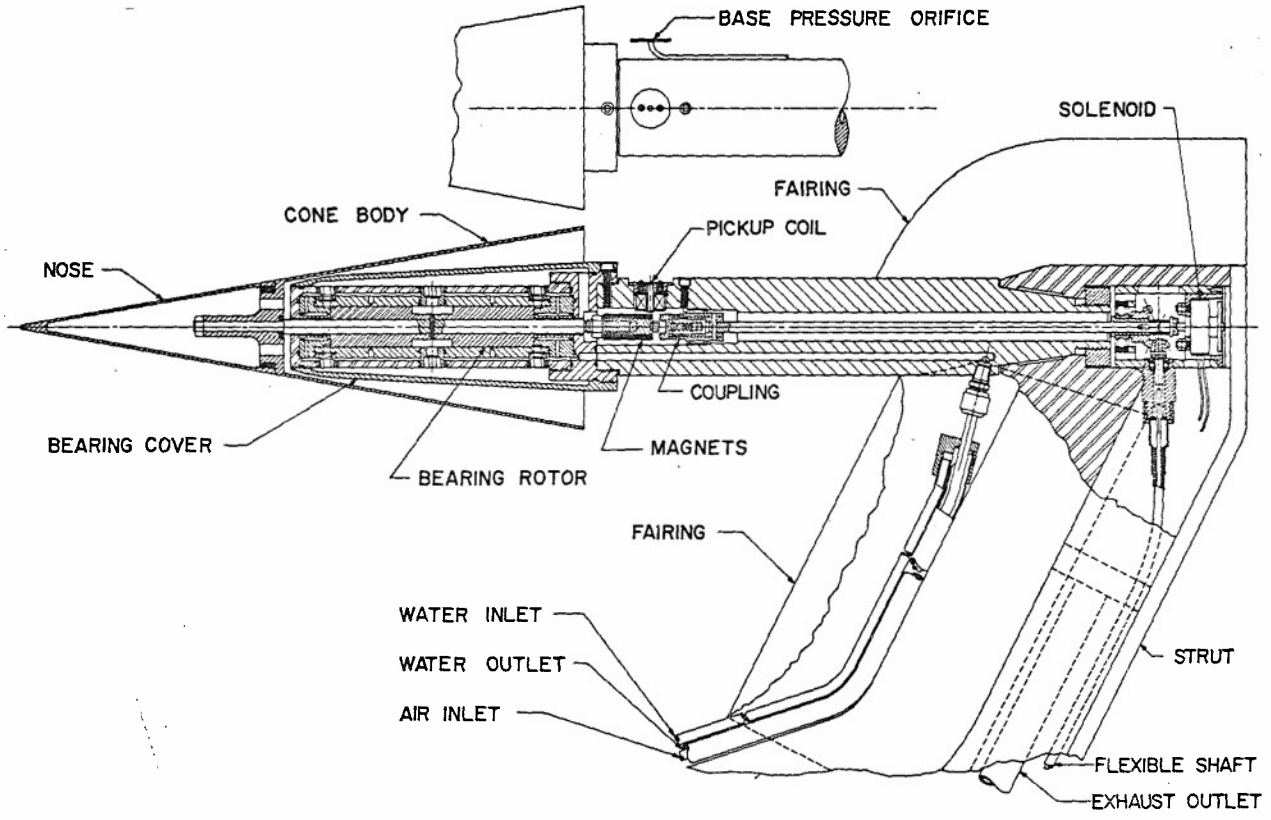

Figure 1. Cone Model - Bearing - Sting - Strut Assembly

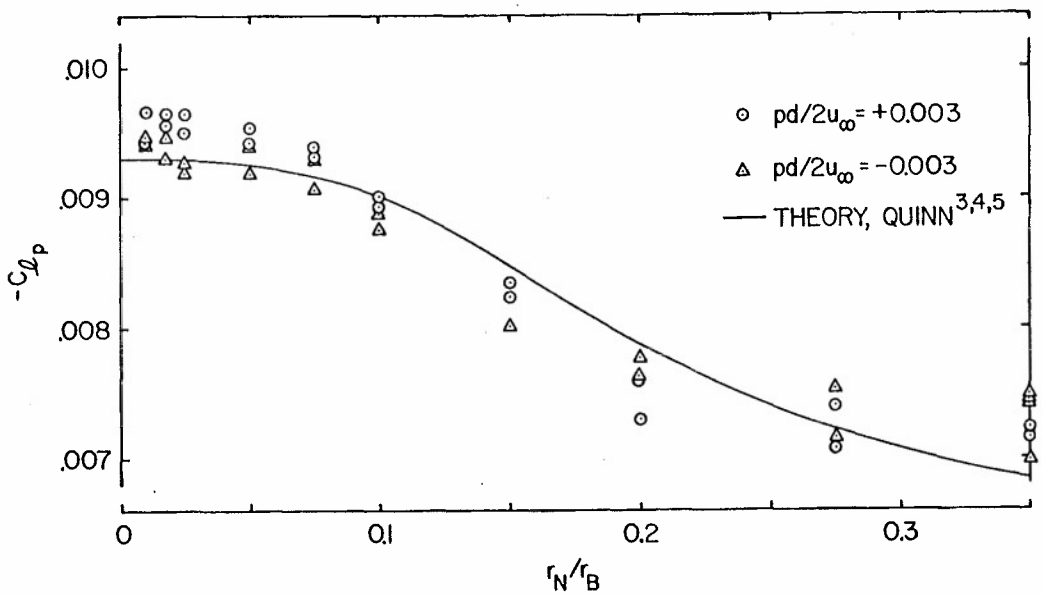

Figure 2. Roll Damping Derivative Versus Nose Bluntness Ratio.
$\theta = 10^o$, $a = 0$, $M_\infty = 14.25$, $P_t = 1615$ psia,
$T_t = 2060^o$ R, $Re_{d,\infty} = 0.241 \times 10^6$

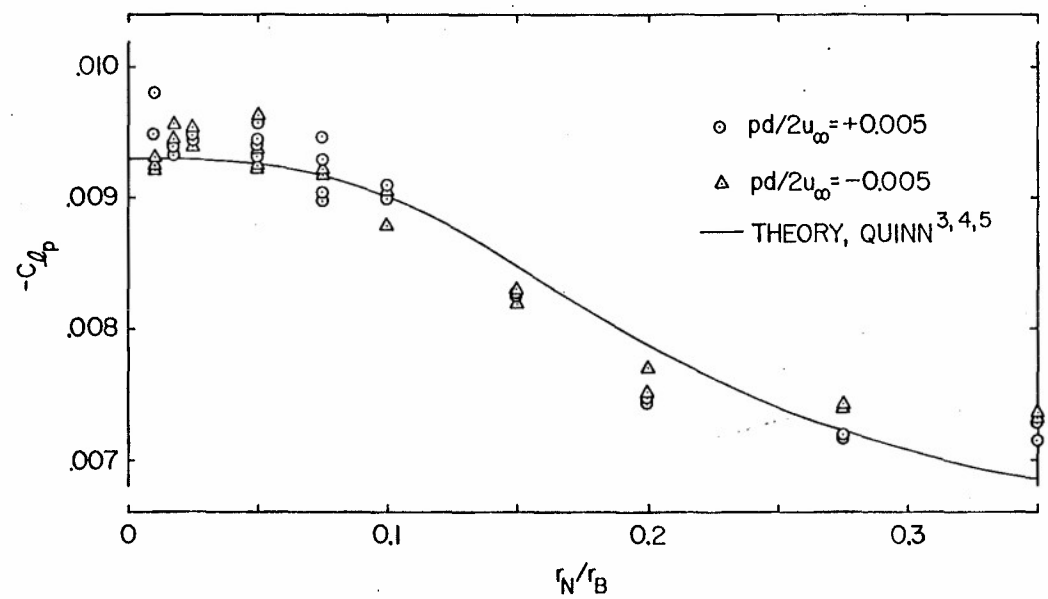

Figure 3. Roll Damping Derivative Versus Nose Bluntness Ratio.
$\theta = 10^o$, $a = 0$, $M_\infty = 14.25$, $P_t = 1615$ psia,
$T_t = 2060^o$ R, $Re_{d,\infty} = 0.241 \times 10^6$

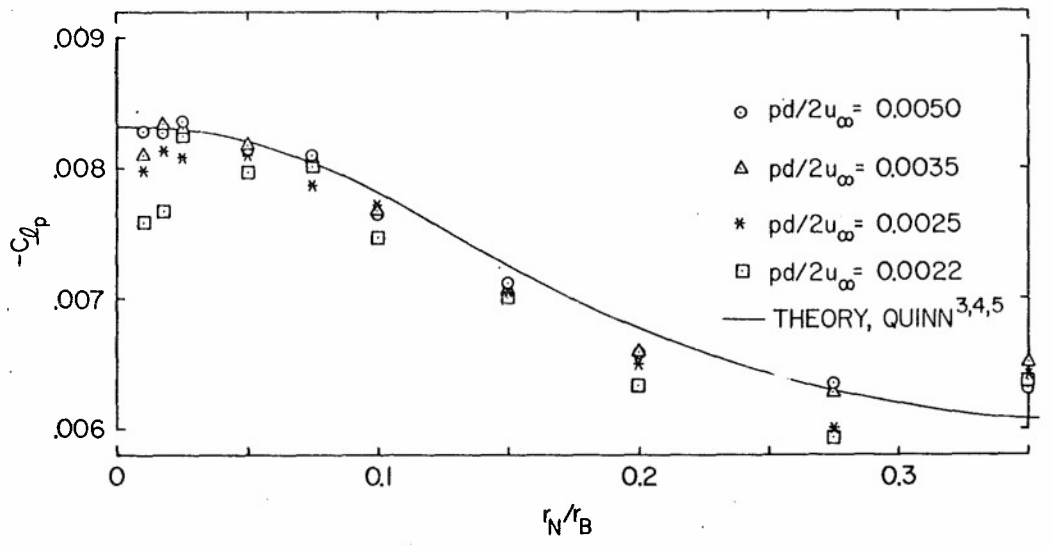

Figure 4. Roll Damping Derivative Versus Nose Bluntness Ratio.
θ = 10°, a = 0, M_∞ = 12.75, P_t = 1185 psia,
T_t = 2010° R, $Re_{d,\infty}$ = 0.260 x 10^6

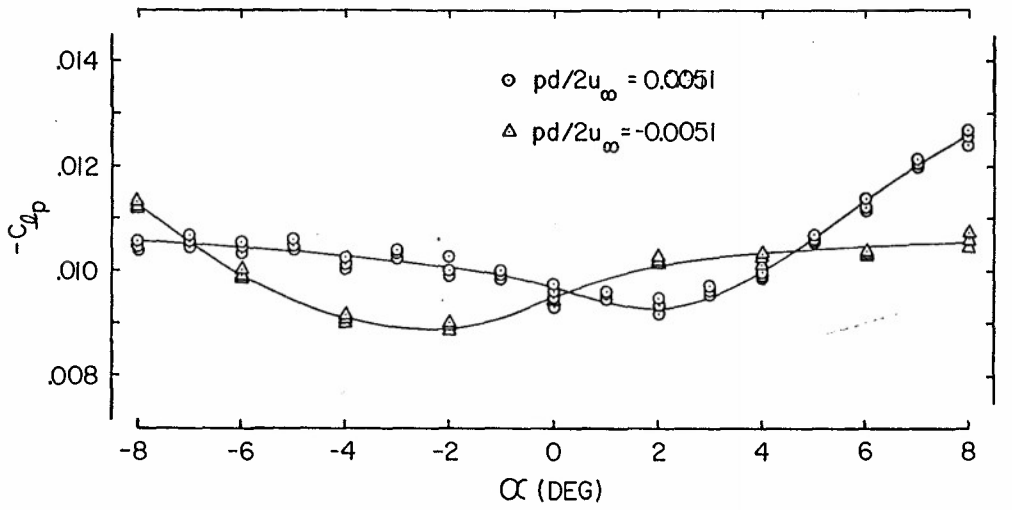

Figure 5. Roll Damping Derivative Versus Angle of Attack.
θ = 10°, r_N/r_B = 0.01, M_∞ = 14.18, P_t = 1505 psia,
T_t = 2050° R, $Re_{d,\infty}$ = 0.227 x 10^6

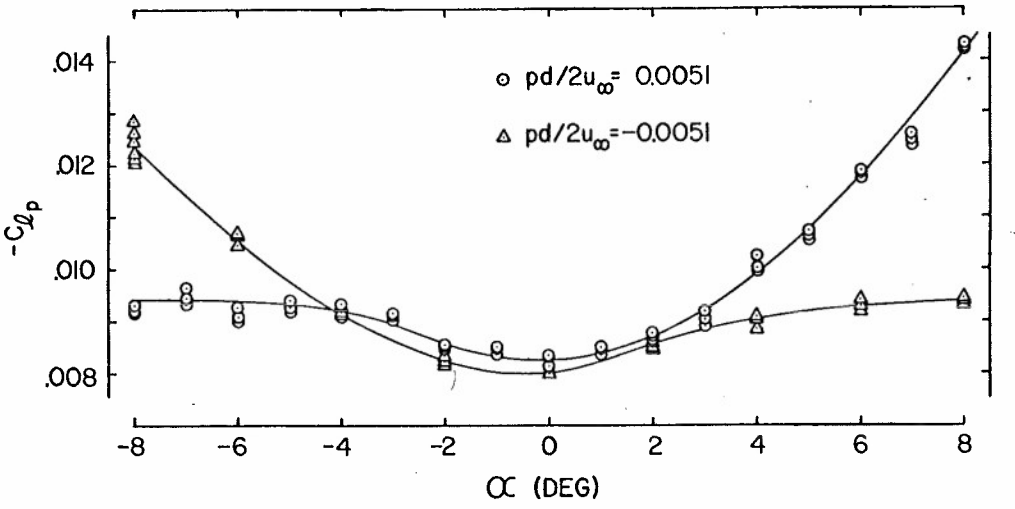

Figure 6. Roll Damping Derivative Versus Angle of Attack.
θ = 10°, r_N/r_B = 0.15, M_∞ = 14.18, P_t = 1505 psia,
T_t = 2050° R, $Re_{d,\infty}$ = 0.227 x 10^6

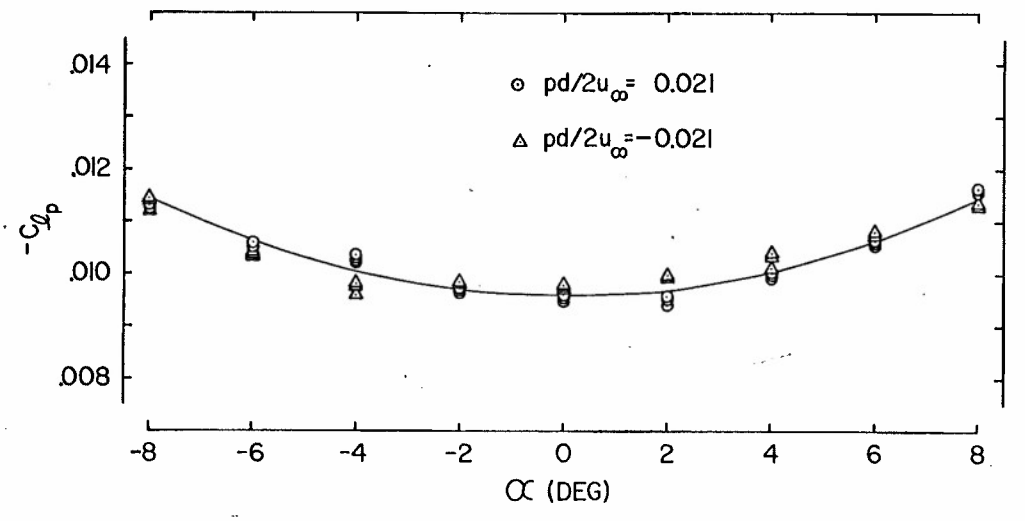

Figure 7. Roll Damping Derivative Versus Angle of Attack.
θ = 10°, r_N/r_B = 0.01, M_∞ = 14.18, P_t = 1507 psia,
T_t = 2060° R, $Re_{d,\infty}$ = 0.225 x 10^6

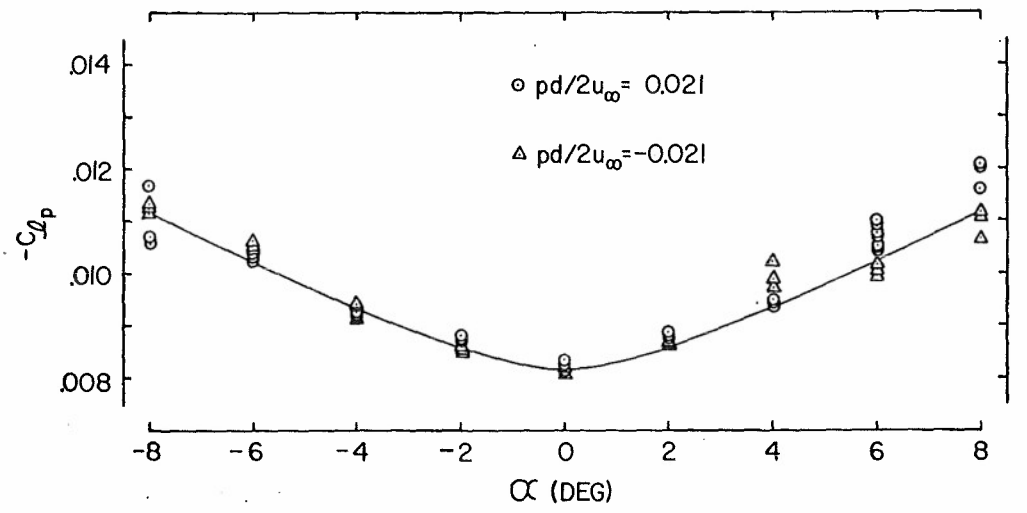

Figure 8. Roll Damping Derivative Versus Angle of Attack.
$\theta = 10^o$, $r_N/r_B = 0.15$, $M_\infty = 14.18$, $P_t = 1507$ psia,
$T_t = 2060^o$ R, $Re_{d,\infty} = 0.225 \times 10^6$

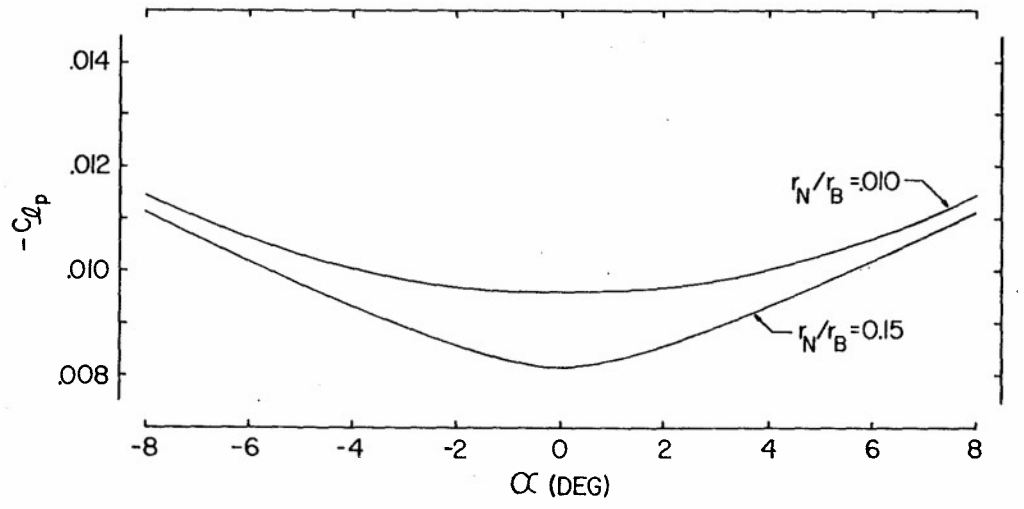

Figure 9. Roll Damping Derivatives Versus Angle of Attack, Compiled from Figures 7 and 8.

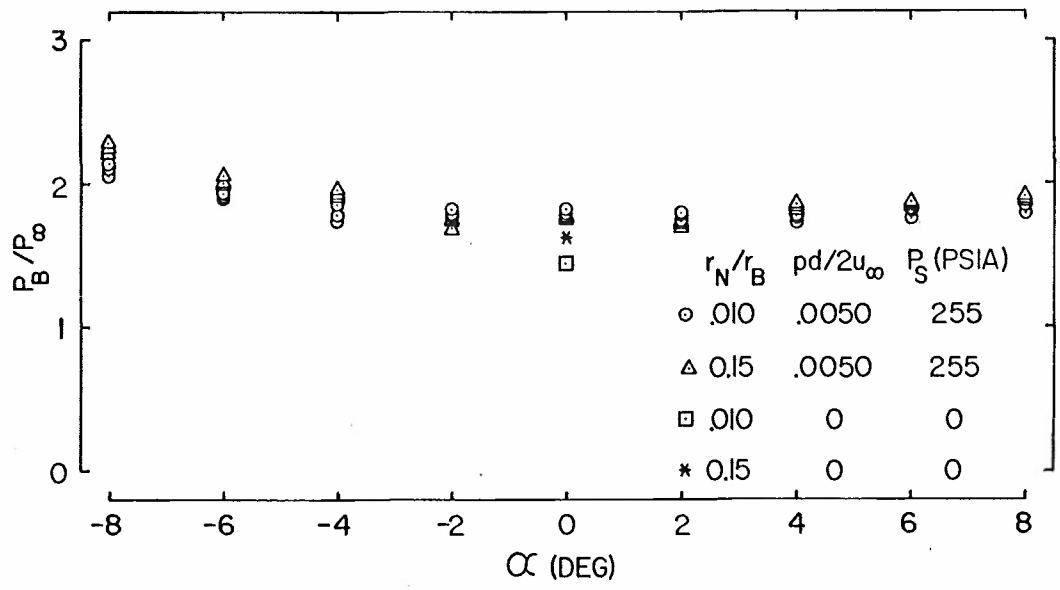

Figure 10. Typical Base Pressures Versus Angle of Attack With and Without Bearing Flow Effect.

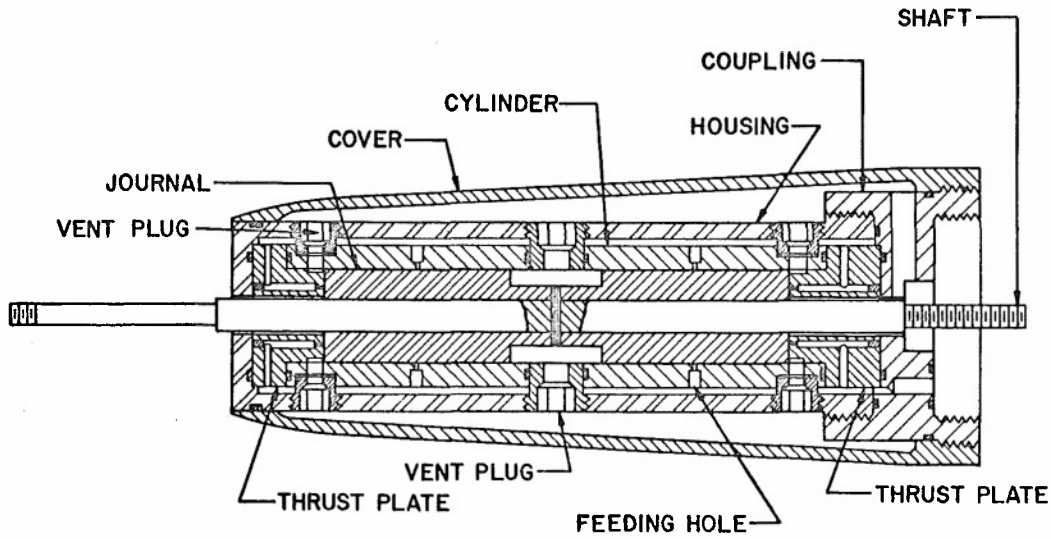

Figure 11. Air Bearing Assembly.

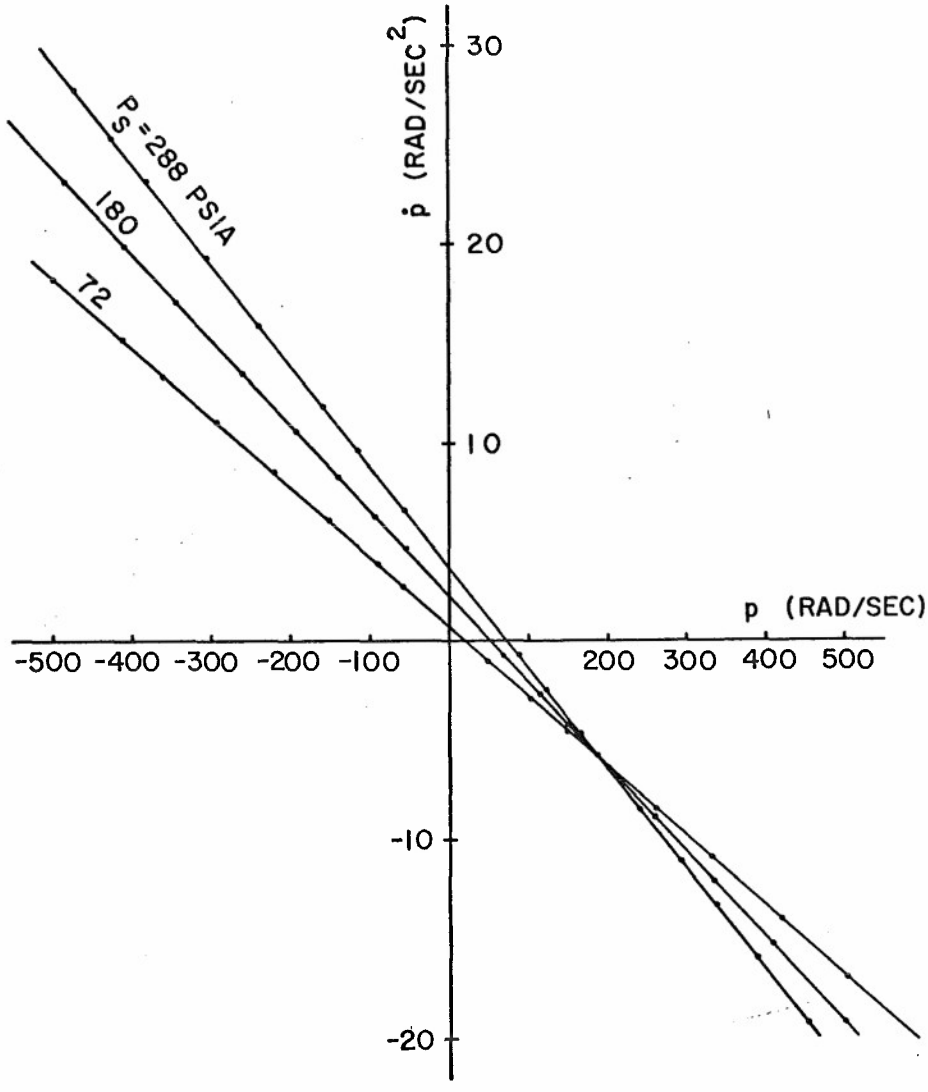

Figure 12. Bearing Characteristics Without Cone Model, Test Cabin Evacuated. Roll Acceleration Versus Roll Rate.

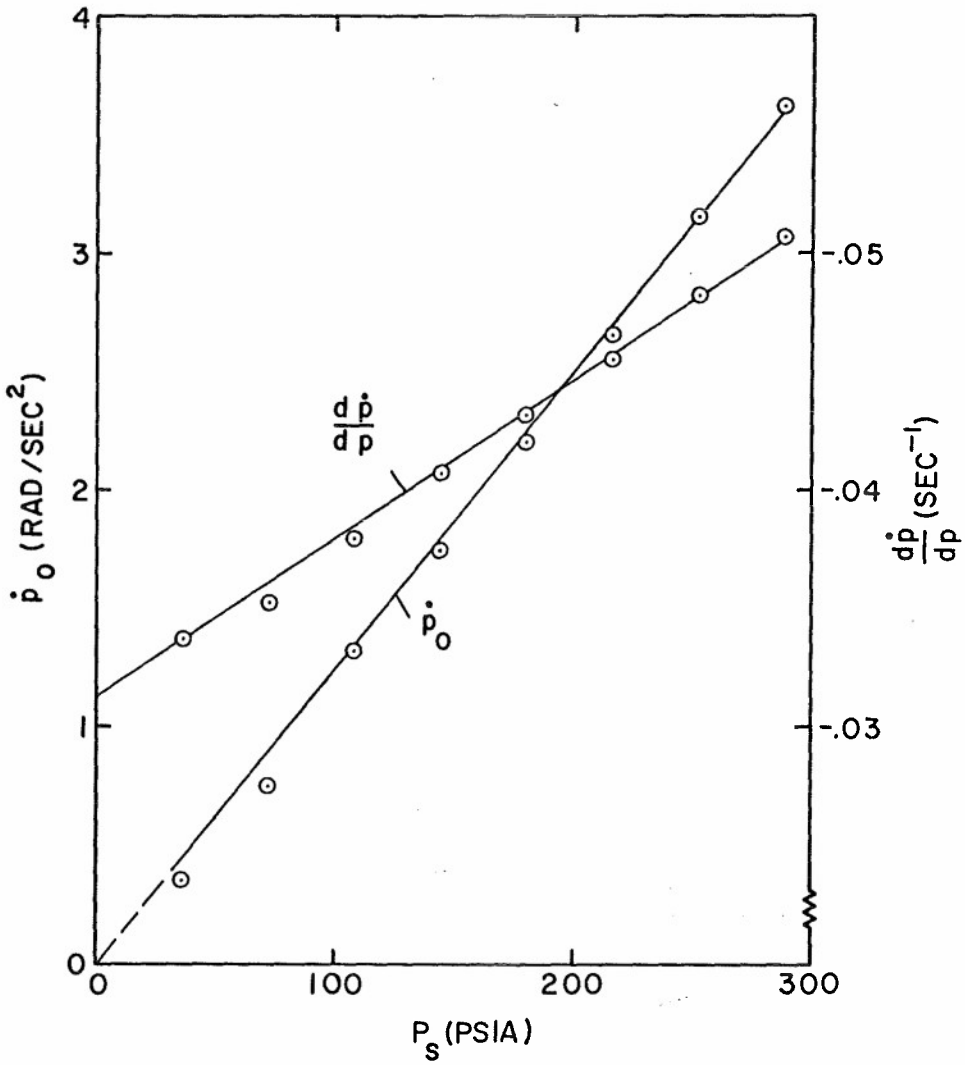

Figure 13. Bearing Characteristics Without Cone Model, Test Cabin Evacuated. Slope of Roll Acceleration With Roll Rate and Roll Acceleration at Zero Roll Rate Versus Supply Pressure.

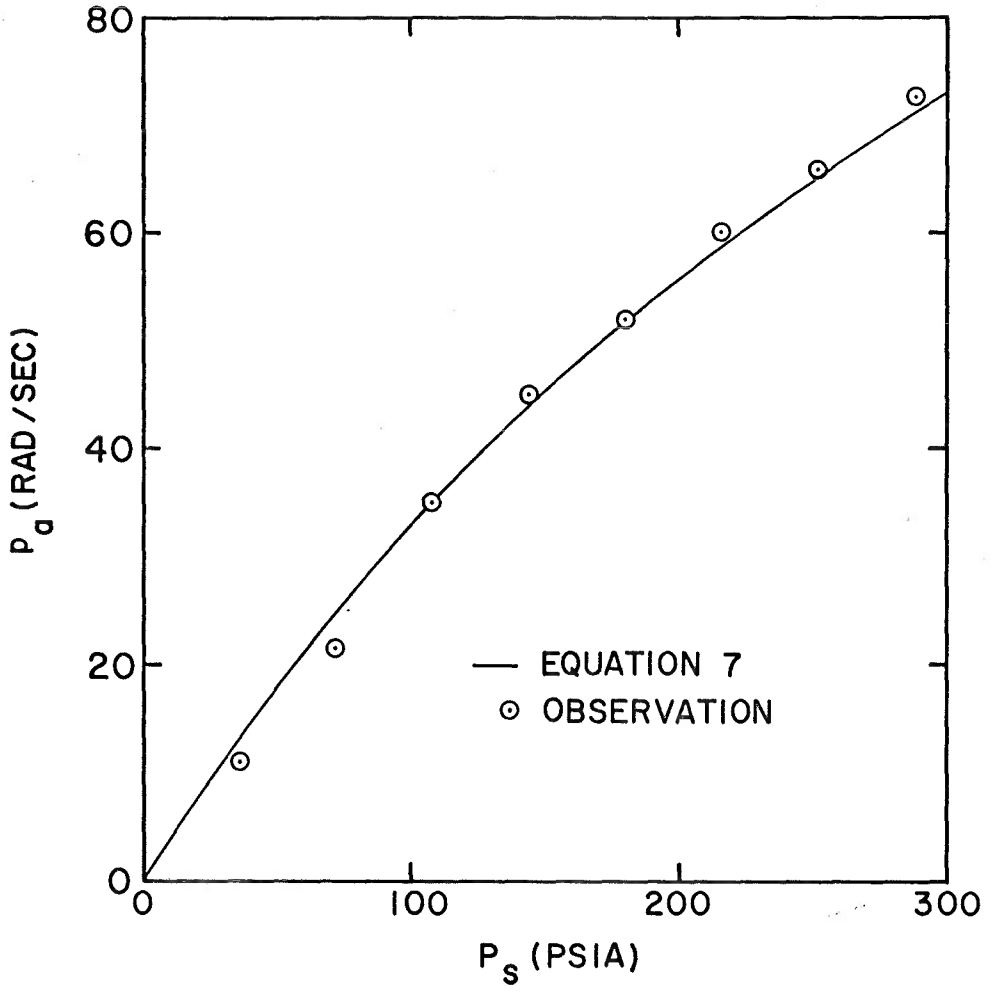

Figure 14. Bearing Characteristics Without Cone Model, Test Cabin Evacuated. Autorotation Roll Rates Versus Supply Pressure.

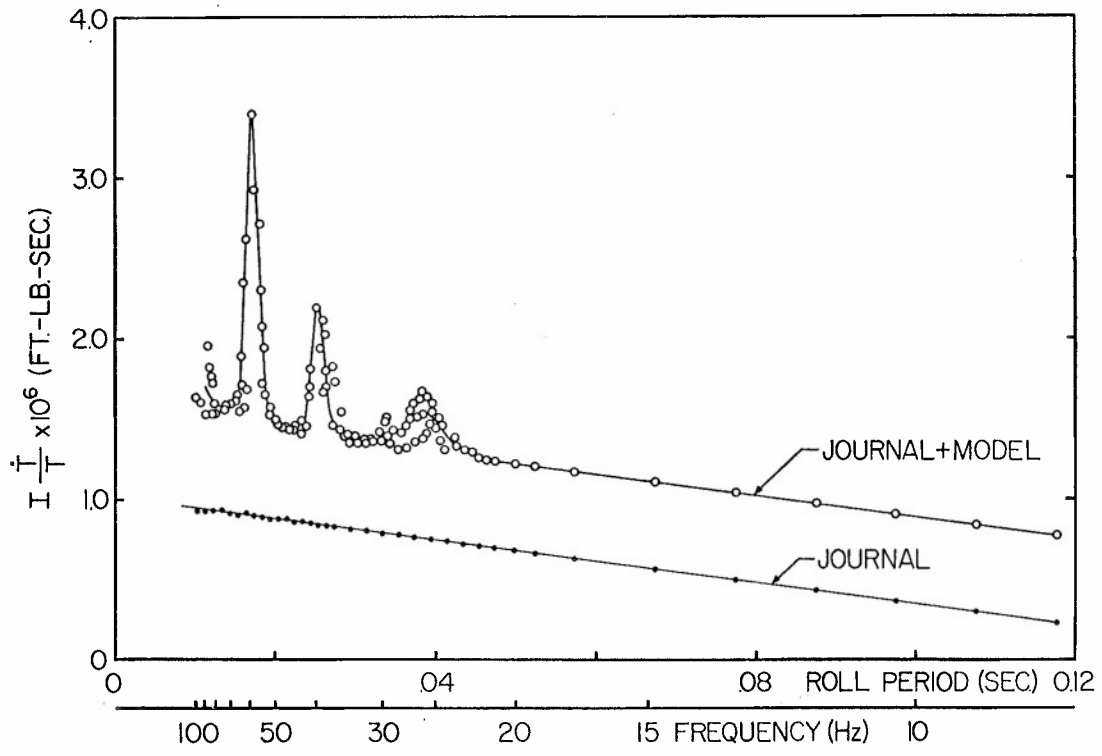

Figure 15. Bearing Performance With and Without Cone Model, Test Cabin Evacuated, No Wind. P_S = 215 psia.

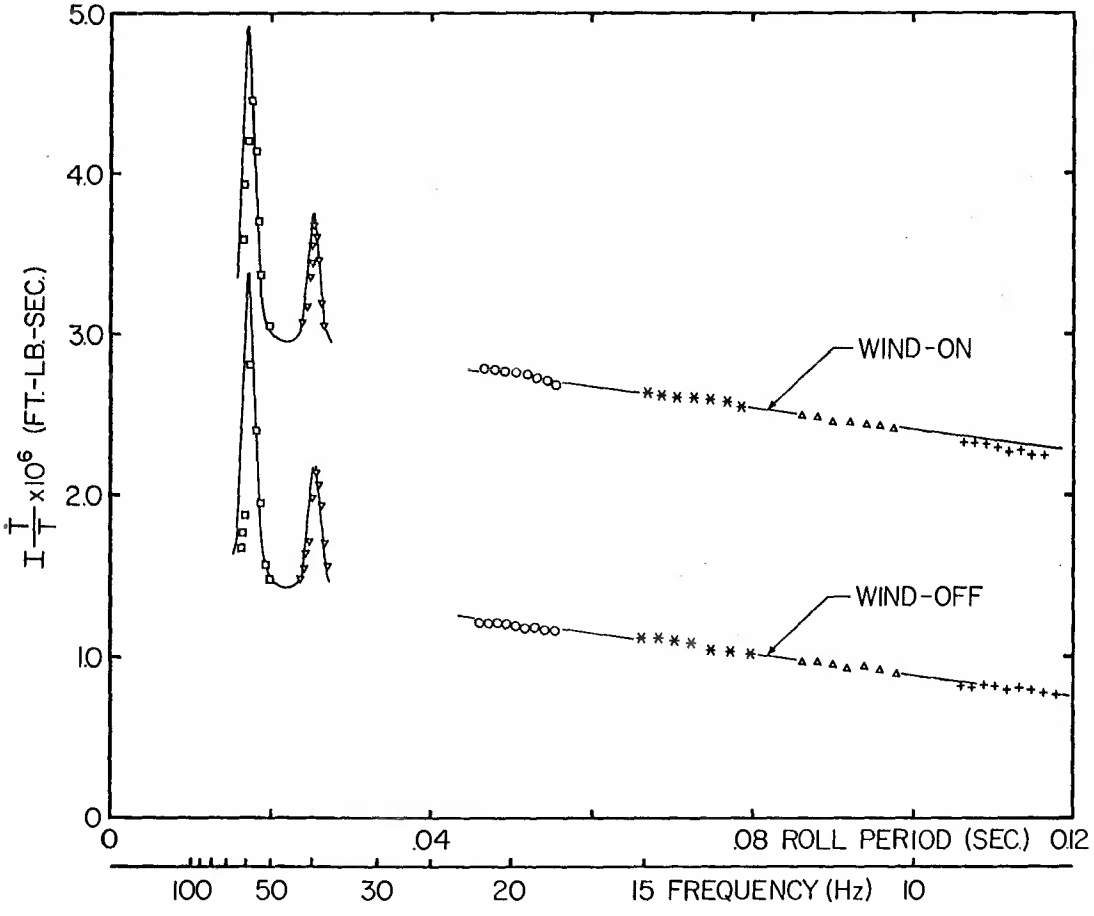

Figure 16. Bearing Performance With Cone Model for Typical Wind-On and Wind-Off Conditions.

UNCLASSIFIED

Security Classification

DOCUMENT CONTROL DATA - R & D

(Security classification of title, body of abstract and indexing annotation must be entered when the overall report is classified)

1. ORIGINATING ACTIVITY (Corporate author)
Aerospace Research Laboratories
Hypersonic Research Laboratory
Wright-Patterson AFB, Ohio 45433

2a. REPORT SECURITY CLASSIFICATION
UNCLASSIFIED

2b. GROUP

3. REPORT TITLE
Hypersonic Wind Tunnel Measurements of Roll Damping Derivatives for Cones

4. DESCRIPTIVE NOTES (Type of report and inclusive dates)
Scientific Interim

5. AUTHOR(S) (First name, middle initial, last name)
Otto Walchner, Frank M. Sawyer, Thomas A. Durham, Capt, USAF

6. REPORT DATE	7a. TOTAL NO. OF PAGES	7b. NO. OF REFS
October 1969	42	10

8a. In-house Research

b. PROJECT NO. 7064-00-01

c. DoD Element 61102F

d. DoD Subelement 681307

9a. ORIGINATOR'S REPORT NUMBER(S)

9b. OTHER REPORT NO(S) (Any other numbers that may be assigned this report)
ARL 69-0170

10. DISTRIBUTION STATEMENT
1. This document has been approved for public release and sale; its distribution is unlimited.

11. SUPPLEMENTARY NOTES
TECH OTHER

12. SPONSORING MILITARY ACTIVITY
Aerospace Research Laboratories (ARR)
Wright-Patterson AFB, Ohio 45433

13. ABSTRACT

The roll damping derivatives, C_{ℓ_p}, for a 10° cone with various nose bluntness ratios were measured in ARL's 20-inch hypersonic wind tunnel at Mach 12.7 and 14.2, $Re_{d_\infty} = 2.5 \times 10^5$, in axial flow and at angles of attack up to ±8 degrees. An air bearing, supporting the model with freedom in roll, was designed specifically for these tests. The bearing performance is described in detail. The measured derivatives compare very favorably with Quinn's laminar roll damping theory for blunted cones in axial flow. A moderate decrease of the magnitude of C_{ℓ_p} results from blunting the nose. At angles of attack, this blunt nose effect diminishes and the blunt cone derivatives approach the sharp cone values with increasing angle of attack. Experimental difficulties at angles of attack were traced to possible free stream deficiencies and were overcome by increasing the model roll rate. No effect of the reduced roll rate on the damping derivative at zero angle of attack was found within the range $pd/2U_\infty = 0.003$ to 0.021.

DD FORM 1 NOV 65 1473

UNCLASSIFIED

Security Classification

Security Classification

14. KEY WORDS	LINK A		LINK B		LINK C	
	ROLE	WT	ROLE	WT	ROLE	WT
Hypersonic Roll Damping Cone Air Bearing						

Security Classification